Pressure broadening and frequency shift of the D_1 and D_2 lines of Rb and K in the presence of ^{3}He and N_2

Kelly A. Kluttz and Todd D. Averett

Department of Physics, College of William and Mary, Williamsburg,Virginia 23185, USA

Brian A. Wolin

Department of Physics, University of Virginia, Charlottesville, Virginia 22904, USA

We report the results of a study of the pressure broadening and resonant frequency shift of the absorption profiles of the D_1 and D_2 lines of Rb and K in the presence of ^{3}He and N_2 gases over a range of number densities. We have also examined the temperature dependence of the broadening and shift over a range of approximately 340 to 400 K. We compare our results for the broadening and shift coefficients for Rb D_1 and D_2 to current values and present coefficients for K D_1 and D_2.

I. INTRODUCTION

The effect of collisions with neutral atoms on atomic spectral lines has been the subject of considerable interest both theoretically and experimentally. A comprehensive review of the development of the theory of line profiles and their experimental measurement is presented in Refs. [1–3]. Well-known consequences of the collision interaction are a broadening of the spectral profile and a shift in the resonance frequency. Both of these quantities have been found to vary with the number density of the surrounding gas [2].

Our interest in the collisional broadening of alkali-metal spectral lines has been motivated by the use of the linewidth as a diagnostic tool for determining the number density of the surrounding gas. In nuclear scattering experiments that require a highly polarized neutron target, glass cells containing a mixture of ^{3}He, N_2, Rb, and K are often used. In a process known as spin-exchange optical pumping (SEOP), Rb atoms are optically pumped and undergo spin exchange with K. The ^{3}He nuclei then become polarized through spin exchange with Rb and K, while N_2 is present to radiationlessly quench the excited alkali-metal atoms. The hybrid mixture of Rb and K enhances the efficiency of the spin-exchange process compared to Rb acting alone [4–6]. Determining the nuclear polarization of these targets requires precise knowledge of the ^{3}He number density. Although the number density of ^{3}He is calculated from the pressure and temperature of the cell when it is filled, this measurement cannot be repeated after the cell is sealed leading to relatively large uncertainty. However, calculating the number density of the gas from the alkali-metal linewidths requires knowledge of the relevant broadening coefficients, or velocity-averaged collisional cross sections.

The most current measurements of the broadening and shift coefficients for Rb with ^{3}He and N_2 [7] are quite accurate, and we provide similar measurements for K in the presence of ^{3}He and N_2. Recent experiments have measured these coefficients for K D_1 up to gas pressures of 80 torr [8], but our ^{3}He target cells are filled to much higher pressures (up to 7600 torr at room temperature). Furthermore, the theory of collisional broadening suggests that the coefficients are temperature dependent, so we provide experimental data to examine this dependence.

II. PRESSURE-BROADENED LINE SHAPE

In the impact approximation, the collision between an atom and a perturbing atom occurs instantaneously, the radiation emitted or absorbed during the collision can be ignored, and the line shape is well described by

$$L(\nu) \propto \frac{\gamma}{\Delta^2 + (\gamma/2)^2}, \tag{1}$$

where $\Delta = \nu - \nu_0 - \delta$ and ν_0 is the natural resonant frequency [2]. The frequency shift δ is due to collisions with the surrounding gas, and $\gamma = \gamma_N + \gamma_c$ is the linewidth (FWHM) which includes the natural linewidth γ_N and γ_c, the collisional broadening contribution. Both δ and γ_c are proportional to the density of the surrounding gas ρ and are sensitive to the details of the interatomic potential difference $V(R)$ between the excited and ground states of the primary atom when interacting with a nearby foreign atom [2].

The impact approximation requires $|\Delta|t_d \ll 1$, where t_d is the collision duration, which for our measurements is typically $\sim 10^{-12}$ s. This approximation works well in the line core, but in the near wings, where $|\Delta| \sim t_d^{-1}$, the line shape begins to deviate from the impact approximation. Walkup *et al.* [9] found that fitting with Eq. (1) results in a linear asymmetry in the near wings not attributable to other sources, e.g., the proximity of the D lines to each other. The physical origin of the asymmetry is the finite duration of the collision, and the Lorentzian profile should be modified to include a detuning-dependent broadening:

$$\gamma = \gamma_N + \gamma_c(\Delta), \tag{2}$$

where the low perturber density regime is assumed. In this regime, the binary collision approximation, where the time between collisions is much longer than the duration of the collision, is valid [10]. This condition can be expressed as $\gamma t_d \ll 1$ since the time between collisions is on the order of $1/\gamma$ [2].

For an alkali metal interacting with a foreign gas, $V(R)$ will be dominated by attractive long-range interactions for atoms with large polarizability such as the heavy noble gases and molecules such as N_2. For lighter gases such as He, the interactions at long range are weaker due to smaller

polarizabilities, and contributions from repulsive short-range interactions must be included [11–13]. For an arbitrary $V(R)$, to first order in Δt_d we can write [1,14],

$$\gamma_c(\Delta t_d) = \gamma_c(0)(1 + a_1 \Delta t_d), \qquad (3)$$

where $\gamma_c(0)$ is the impact approximation result ($t_d = 0$), and a_1 is a constant that depends on the choice of $V(R)$.

To determine an expression for $\gamma_c(\Delta t_d)$, Walkup *et al.* [10] calculated the line shape using a long-range (attractive) van der Waals potential difference, $V(R) = -C_6 R^{-6}$, where C_6 is a positive constant. They assume straight-line trajectories for the perturbing atoms, i.e., the separation distance is $R(t) = \sqrt{b^2 + v^2(t - t_0)^2}$ where b is the impact parameter, v is the perturber velocity, and t_0 is the time of closest approach. The broadening is then given by

$$\gamma_c(\Delta t_d) = \rho v_{\text{th}} 8\pi R_{\text{th}}^2 I(\Delta t_d), \qquad (4)$$

where $v_{\text{th}} = \sqrt{2kT/\mu}$ is the thermal velocity, $R_{\text{th}} = (C_6/v_{\text{th}})^{1/5}$ is the collision radius, and t_d is defined as $t_d = R_{\text{th}}/v_{\text{th}}$. The dimensionless quantity $I(\Delta t_d)$ was calculated numerically for the entire line shape. In the region $-1.5 < \Delta t_d < 0.5$, the numerical result agrees remarkably well with a Taylor's expansion of $I(\Delta t_d)$ to first order in Δt_d. This region covers much of the transition between the impact region and the far wings and is the region of interest for this work. The Taylor's expansion is given by

$$I(\Delta t_d) \simeq 0.3380 - 0.2245 \times 2\pi \Delta t_d. \qquad (5)$$

Substituting Eq. (5) into (4) gives the following expression for the broadening:

$$\gamma_c(\Delta t_d) = \gamma_c(0)(1 - 0.6642 \times 2\pi \Delta t_d). \qquad (6)$$

Note that for a repulsive potential difference, the signs in Eqs. (5) and (6) will be positive [10]. Since $|\Delta| t_d, \gamma t_d$ and γ_N/γ_c are $\ll 1$ for our experimental conditions, the line shape is well described by [10]

$$L(\Delta) \propto \frac{\gamma_c(\Delta t_d)}{\Delta^2 + [\gamma_c(0)/2]^2}. \qquad (7)$$

III. EXPERIMENTAL TECHNIQUE

Figure 1 shows the experimental setup. A glass cell containing a mixture of Rb and K along with either ^{3}He or N$_2$ was held inside an oven and heated to vaporize the alkali metal. A tunable Ti:sapphire laser was used to collect spectroscopic data for the D_1 and D_2 lines of the alkali metals. The transmission of laser light through the cell was monitored while the laser wavelength was scanned across the D_1 and D_2 transitions. A series of scans were performed at different ^{3}He and N$_2$ number densities over a range of temperatures. The absorption profiles were fit with the modified Lorentzian function, Eq. (7), and the linewidth and central frequency were extracted and examined as a function of ^{3}He or N$_2$ number density and temperature.

A. Cell preparation

The cell constructed for this experiment was a 2-in.-diameter Pyrex sphere with a narrow stem connected to

FIG. 1. Setup for collecting pressure broadening data. Solid lines indicate the laser path; dashed lines are electronic connections. The first beam splitter is polarizing (PBS), while the second is nonpolarizing (NPBS).

a stainless steel valve by a glass-to-Kovar seal. The valve allowed the cell to be filled with either ^{3}He or N$_2$ to a specified pressure, pumped out, and refilled multiple times. The alkali metal was mixed such that the ratio of Rb to K would be approximately 1:1 at our operating temperature. Prior to filling, the cell was connected to the vacuum system, periodically heated with a cool flame, and evacuated to 6×10^{-8} torr. After the hybrid alkali metal was moved into the spherical portion of the cell by distillation with a flame, the cell was detached from the vacuum system and sealed.

A filling system allowed either ^{3}He or N$_2$ to be introduced into the cell while the gas pressure and temperature were measured. The gas density was calculated using the ideal gas law and has an uncertainty of $\pm 1\%$. The procedure for collecting data was to fill the cell to a specific density of ^{3}He or N$_2$, collect spectroscopic data across the D_1 and D_2 transitions for a range of temperatures, and then release some amount of the gas and repeat the measurements at the same temperatures. This process was repeated until the pressure in the cell decreased to approximately atmospheric pressure at room temperature.

The ^{3}He number densities ranged from [^{3}He] = 1.00 ± 0.01 to 6.02 ± 0.06 amagat (amg), while the N$_2$ number densities were [N$_2$] = 2.50 ± 0.03, 1.87 ± 0.02, and 0.92 ± 0.01 amg. Note that 1 amg = 2.69×10^{25} m^{-3}. Higher number densities of N$_2$ were not used because the low-density approximation fails at a critical density of [N$_2$] = 5.5 amg, where the line shape begins to deviate significantly from Eq. (7) [7].

B. Data acquisition

Data were first collected with N$_2$ and then the cell was pumped out and refilled with ^{3}He. During the spectroscopic scans, the temperature of the oven was held constant and controlled by a variable power supply. The temperatures typically ranged from 333 to 403 K with data collected at 10 K increments. However, the signal-to-noise ratio for the data taken at 333 K was too low due to weak absorption,

so these data were excluded from the final analysis. The temperatures of the oven and several points on the cell were monitored with thermocouples. The system was allowed to equilibrate each time the oven temperature was adjusted. The cell temperature was measured with an uncertainty of ± 2 K. The cell was positioned to avoid sinusoidal modulation of the absorption profile due to optical interference from the glass and to minimize any overall slope across the wavelength range [15,16]. The oven's entrance and exit windows were removed to eliminate additional interference; their absence did not compromise the temperature stability. Scans were also made with an empty cell at room temperature and showed no frequency dependence in the background.

The wavelength of the single-frequency Ti:sapphire laser is tunable from 700 to 1000 nm, which allowed the D_1 and D_2 transitions for both Rb and K to be probed. An optical isolator was positioned after the laser to prevent back-reflections into the laser cavity. The portion of the beam reflected from the front of the isolator was coupled into a multimode optical fiber feeding a wavelength meter, which is accurate to ± 0.1 ppm over the typical time of a line-shape measurement and a long-term variation of ± 0.75 ppm. The half-wave plates before and after the isolator control the intensity of light sent to the wavelength meter and to the experiment, respectively. The light transmitted through the polarizing beam splitter was coupled into a single-mode optical fiber with the output at an optical chopper, which modulated the beam at 331 Hz. A second beam splitter (nonpolarizing) directed the transmitted beam into the oven where it passed through the cell while the reflected beam bypassed the oven to become a reference to account for laser power fluctuations. The photodiode at the end of each path was connected to one of two lockin amplifiers referenced to the chopper frequency. The linearity of the photodiodes across the range of laser power used was confirmed to better than 1% using a calibrated power meter without the cell in place. Because the photodiode signals were locked to the chopper frequency, any dc background in the photodiodes contributed negligibly to the measured signals. The lockin outputs were digitized by an analog-to-digital converter (ADC), which was read by the data acquisition computer, and the ratio of the transmitted signal to the reference signal was plotted as a function of wavelength.

IV. FITTING THE PROFILES

Using Beer's law, the intensity transmitted through the cell is given by

$$I_t(\nu) = I_0(\nu) \exp[-[A]\sigma(\nu)L], \tag{8}$$

where I_0 is the incident intensity, $[A]$ is the alkali-metal density, and L is the path length through the cell. The absorption cross section $\sigma(\nu)$ is given by Eq. (7):

$$\sigma(\nu) = \left(\frac{\sigma_0}{2\pi}\right)\frac{\gamma\,(1 + 0.6642 \times 2\pi\,\Delta t_d)}{\Delta^2 + (\gamma/2)^2}, \tag{9}$$

where the linewidth (FWHM) is $\gamma = \gamma_c(0)$.
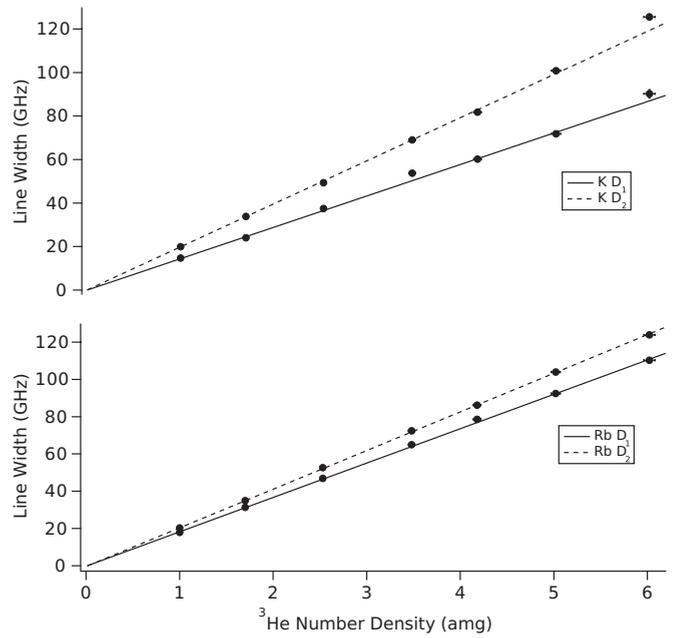

FIG. 2. Measured linewidths for D_1 and D_2 for Rb and K in the presence of ^{3}He at 363 ± 2 K with fits from Eq. (14).

Integrating the cross section over all frequencies gives [7]

$$\int_0^\infty \sigma(\nu)d\nu = \sigma_0 = \pi r_e c f, \tag{10}$$

where r_e is the classical electron radius, c is the speed of light, and f is the oscillator strength.

At the reference and transmission photodiodes we measure

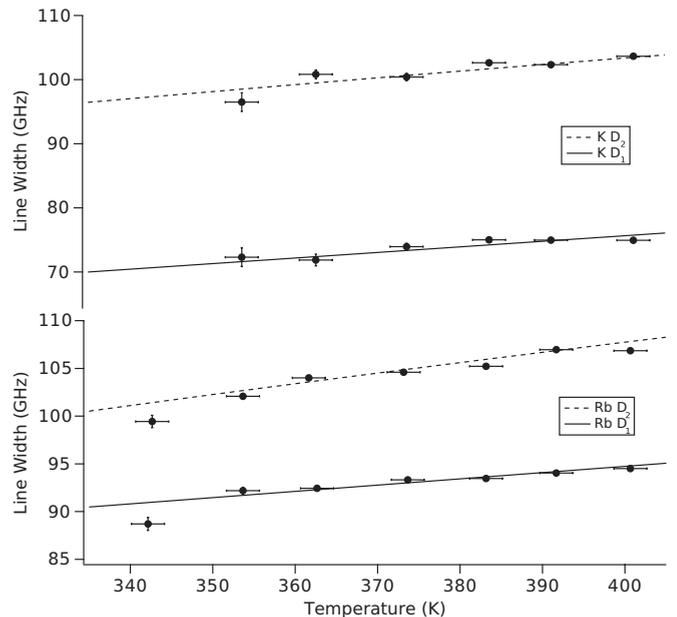$$S_r(\nu) = G_r I_0(\nu) \quad \text{and} \quad S_t(\nu) = G_t I_t(\nu), \tag{11}$$

FIG. 3. Measured linewidths for D_1 and D_2 for Rb and K as a function of temperature for a ^{3}He density of $\rho = 5.02 \pm 0.05$ amg with linear fits from Eq. (14).

TABLE I. Fits to the measured linewidths γ in the presence of ^{3}He as a function of density and temperature. Reduced chi-squared values for the fits are also listed.

	α (GHz/amg)	n	β (GHz)	$\tilde{\chi}^2$
Rb D_1	18.31 ± 0.07	0.26 ± 0.04	-0.19 ± 0.13	1.1
Rb D_2	20.51 ± 0.08	0.39 ± 0.04	-0.35 ± 0.15	1.0
K D_1	14.26 ± 0.09	0.44 ± 0.06	0.04 ± 0.11	1.9
K D_2	19.59 ± 0.10	0.39 ± 0.05	0.11 ± 0.13	1.5

where G is the gain of each circuit. Taking the natural log of the ratio of the signals gives

$$\ln\left(\frac{S_t}{S_r}\right) = \left(\frac{-\gamma[A]\sigma_0 L}{2\pi}\right)\frac{(1 + 0.6642 \times 2\pi\,\Delta t_d)}{\Delta^2 + (\gamma/2)^2}$$
$$+ \ln\left(\frac{G_r}{G_t}\right). \tag{12}$$

For fitting the data (both He and N$_2$), we write Eq. (12) as

$$y(\nu) = \frac{A[1 + 0.6642 \times 2\pi(\nu - \nu_c)t_d]}{(\nu - \nu_c)^2 + (\gamma/2)^2} + y_0, \tag{13}$$

where $\nu_c = \nu_0 + \delta$ is the resonant frequency. The last term y_0 is the transmitted to incident intensity ratio in the absence of absorption and was constant to much better than 1% over the measured frequency range. The free parameters of the fit are A, ν_c, t_d, γ, and y_0. The log of the signal ratio was plotted as a function of frequency and the nonlinear Levenberg-Marquardt algorithm was employed to optimize the five parameters in Eq. (13) to minimize χ^2. For Rb, the ground-state hyperfine splitting is larger than 3 GHz for both isotopes [17], so we fit to a sum of four equations with the form of Eq. (13); one for each ground state of each isotope. Each term was weighted with the natural abundance of ^{85}Rb and ^{87}Rb. Fitting to a single Lorentzian overestimates the linewidth. The hyperfine splitting is less than 1 GHz for the ground state of the abundant isotopes of K and for the excited states of both alkali metals. Values for δ were obtained by subtracting the natural resonant frequencies ν_0 taken from [18–21].

V. ANALYSIS AND DISCUSSION

A. Results

Plotting γ and δ as a function of number density at fixed temperature consistently showed linear behavior as seen in [7,15]. Examples of this behavior for ^{3}He are shown in Fig. 2, which shows γ vs ρ at 363 ± 2 K. Figure 3 shows an example of γ vs T for ^{3}He at $\rho = 5.02 \pm 0.05$ amg. Uncertainties

TABLE II. Fits to the measured frequency shifts δ in the presence of ^{3}He as a function of density and temperature. Reduced chi-squared values for the fits are also listed.

	α' (GHz/amg)	n'	β' (GHz)	$\tilde{\chi}^2$
Rb D_1	5.46 ± 0.05	0.38 ± 0.06	0.24 ± 0.13	0.5
Rb D_2	0.63 ± 0.04	1.42 ± 0.43	0.20 ± 0.12	1.4
K D_1	1.36 ± 0.06	-0.14 ± 0.36	0.28 ± 0.12	1.7
K D_2	0.69 ± 0.06	-2.04 ± 0.72	0.02 ± 0.12	1.4

TABLE III. Same as Table I, but for N$_2$.

	α (GHz/amg)	n	β (GHz)	$\tilde{\chi}^2$
Rb D_1	17.41 ± 0.13	0.03 ± 0.06	-0.49 ± 0.18	1.6
Rb D_2	18.83 ± 0.14	-0.19 ± 0.08	-2.35 ± 0.19	14.0
K D_1	18.30 ± 0.21	0.59 ± 0.10	-0.32 ± 0.21	2.6
K D_2	17.43 ± 0.16	0.35 ± 0.08	0.31 ± 0.17	2.5

shown include uncertainties in the fill density, cell temperature, laser frequency, and fits to the line shapes.

The measured linewidths and frequency shifts were fit as a function of density ρ and temperature T with the following equations:

$$\gamma(\rho,T) = \alpha\rho\left(\frac{T}{T_0}\right)^n + \beta, \tag{14}$$

$$\delta(\rho,T) = \alpha'\rho\left(\frac{T}{T_0}\right)^{n'} + \beta', \tag{15}$$

where $T_0 = 353$ K.

The coefficients from the fits are presented in Tables I and II for ^{3}He and Tables III and IV for N$_2$. Note that the coefficients α' describing the frequency shifts for ^{3}He are positive and for N$_2$ are negative, consistent with previous results [7] and predictions [12,13] (for He). A positive frequency shift for ^{3}He indicates that the potential difference is repulsive. Values for β and β' are generally consistent with zero as expected.

The temperature dependence of γ and δ is expected to be $n = (p-3)/2(p-1)$ for any potential of the form $1/R^p$ [13, 22]. The Lennard-Jones potential difference, which is often used to model He, includes a repulsive short-range contribution [13] and is given by

$$V(R) = -C_6 R^{-6} + C_{12} R^{-12}, \tag{16}$$

where C_{12} is a positive constant. Thus we would expect $n = 0.3$ for the C_6 term and $n = 0.409$ for the C_{12} term. Our results do not show consistent behavior for the temperature dependence. This is possibly due to the rather limited range of temperatures measured.

B. Comparison of results

Table V lists the broadening and frequency shift coefficients obtained for Rb in the presence of ^{3}He and N$_2$ found by Romalis et al. [7]. In their work, the temperature dependence of the broadening and shift coefficients was measured for ^{4}He and then scaled by the ratio of the ^{3}He to ^{4}He reduced masses to give the temperature dependence of the ^{3}He coefficients. Their data for temperature dependence were fit to a function of the

TABLE IV. Same as Table II, but for N$_2$.

	α' (GHz/amg)	n'	β' (GHz)	$\tilde{\chi}^2$
Rb D_1	-7.65 ± 0.14	0.44 ± 0.12	0.25 ± 0.25	0.2
Rb D_2	-5.70 ± 0.14	0.48 ± 0.21	0.23 ± 0.25	0.2
K D_1	-6.03 ± 0.18	1.26 ± 0.24	0.12 ± 0.25	1.6
K D_2	-5.04 ± 0.15	0.72 ± 0.22	0.05 ± 0.23	1.0

TABLE V. Rb D_1 and D_2 broadening and frequency shift coefficients and temperature dependence from Romalis *et al.* [7].

He	α, α' (GHz/amg)	n, n'
D_1 width	18.7 ± 0.3	0.05 ± 0.05
shift	5.64 ± 0.15	1.1 ± 0.1
D_2 width	20.8 ± 0.2	0.53 ± 0.06
shift	0.68 ± 0.05	1.6 ± 0.4
N$_2$	α, α' (GHz/amg)	n, n'
D_1 width	17.8 ± 0.3	
shift	-8.25 ± 0.15	
D_2 width	18.1 ± 0.3	
shift	-5.9 ± 0.1	

form of Eqs. (14) and (15) with $T_0 = 353$ K and $\beta, \beta' = 0$. The temperature dependence of the width and shift in the presence of N$_2$ was not presented in their results. Our results for α and α' are in general agreement with their results. Results for temperature dependence were less consistent.

VI. CONCLUSION

We have investigated the effect of collisions on the line shapes of the D_1 and D_2 transitions of vapors of Rb and K in the presence of ^{3}He and N$_2$ gases. The dependence of the linewidth and central frequency shift on both the surrounding gas number density and temperature were measured. Our results show a linear dependence on the density in agreement with previous measurements. Assuming a T^n dependence, we find that the broadening and shift are not consistently described by any specific values of n across the temperature range measured. These results allow us to accurately determine the density of surrounding ^{3}He or N$_2$ gases by observing the modification to the atomic line shapes of Rb and K.

ACKNOWLEDGMENTS

[1] J. F. Kielkopf, J. Phys. B **9**, 160 (1976).

[2] N. Alland and J. F. Kielkopf, Rev. Mod. Phys. **54**, 1103 (1982).

[3] J. Szudy and W. E. Baylis, Phys. Rep. **266**, 127 (1996).

[4] A. B. Baranga, S. Appelt, M. V. Romalis, C. J. Erickson, A. R. Young, G. D. Cates, and W. Happer, Phys. Rev. Lett. **80**, 2801 (1998).

[5] E. Babcock, I. Nelson, S. Kadlecek, B. Driehuys, L. W. Anderson, F. W. Hersman, and T. G. Walker, Phys. Rev. Lett. **91**, 123003 (2003).

[6] W. C. Chen, T. R. Gentile, T. G. Walker, and E. Babcock, Phys. Rev. A **75**, 013416 (2007).

[7] M. V. Romalis, E. Miron, and G. D. Cates, Phys. Rev. A **56**, 4569 (1997).

[8] G. A. Pitz *et al.*, J. Quant. Spectrosc. Radiat. Transfer **113**, 387 (2012).

[9] R. E. Walkup, A. Spielfiedel, and D. E. Pritchard, Phys. Rev. Lett. **45**, 986 (1980).

[10] R. Walkup, B. Stewart, and D. E. Pritchard, Phys. Rev. A **29**, 169 (1984).

[11] J. F. Kielkopf, J. Chem. Phys. **61**, 4733 (1974).

[12] J. F. Kielkopf, J. Phys. B: At. Mol. Phys. **9**, L547 (1976).

[13] A. Bielski, R. Bobkowski, and J. Szudy, Astron. Astrophys. **208**, 357 (1989).

[14] J. Szudy and W. E. Baylis, J. Quant. Spectrosc. Radiat. Transfer **17**, 681 (1977).

[15] P. Mastromarino, C. Otey, D. Pripstein, and E. Hughes, Nucl. Instrum. Methods B **194**, 69 (2002).

[16] J. Singh, Ph.D. thesis, University of Virginia, 2010.

[17] E. Arimondo, M. Inguscio, and P. Violino, Rev. Mod. Phys. **49**, 31 (1977).

[18] J. Ye, S. Swartz, P. Jungner, and J. L. Hall, Opt. Lett. **21**, 1280 (1996).

[19] G. P. Barwood, P. Gill, and W. R. C. Rowley, Appl. Phys. B **53**, 142 (1991).

[20] A. Banerjee, D. Das, and V. Natarajan, Europhys. Lett. **65**, 172 (2004).

[21] S. Falke, E. Tiemann, C. Lisdat, H. Schnatz, and G. Grosche, Phys. Rev. A **74**, 032503 (2006).

[22] W. R. Hindmarsh, A. D. Petford, and G. Smith, Proc. R. Soc. Lond. A **297**, 296 (1967).